Astronomy 6570
Physics of the Planets

Planetary Rotation, Figures, and Gravity Fields

Topics to be covered:

1. Rotational distortion & oblateness
2. Gravity field of an oblate planet
3. Free & forced planetary precession

Rotational distortion

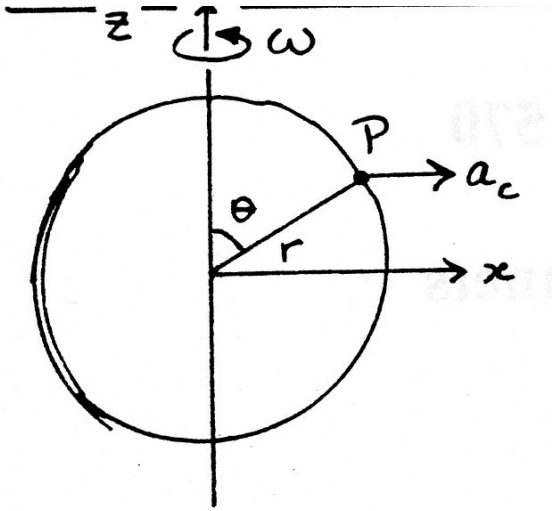

Consider a spherical, rigid planet rotating at an angular rate ω.

Point P on the surface experiences a centrifugal acceleration:

$$\underset{\sim}{a}_c = \omega^2 r \sin\theta \, \hat{x}$$
$$= \omega^2 x \quad \hat{x}$$

By symmetry, a similar point located on the surface in the yz plane feels an acceleration

$$\underset{\sim}{a}_c = \omega^2 y \quad \hat{y},$$

so that an arbitrary point on the surface at position (x, y, z) feels an acceleration

$$\underset{\sim}{a}_c = \omega^2 \left(x \, \hat{x} + y \, \hat{y} \right)$$

It is convenient to think of this centrifugal acceleration in terms of a centrifugal potential, V_c, such that

$$\underset{\sim}{a}_c = -\Delta V_c.$$

Clearly we must have

$$V_c = -\frac{1}{2}\omega^2 \left(x^2 + y^2 \right)$$
$$= -\frac{1}{2}\omega^2 r^2 \sin^2\theta$$

Now consider an ocean on the surface of the rotating planet. the fluid experiences a total potential

$$V_T\left(r,\theta\right) = -\frac{GM}{r} + V_c\left(r,\theta\right).$$

In equilibrium, the surface of a fluid must lie on an equi-potential surface (i.e., the surface is locally perpendicular to the net gravitational and centrifugal acceleration). Assuming the distortion of the ocean surface from a sphere to be small, we write

$$r_{ocean} = a + \delta r\left(\theta\right), \quad \left(a = r_{equator}\right)$$

so $$V_T\left(surface\right) \simeq -\frac{GM}{a} + \frac{GM}{a^2}\,\delta r - \frac{1}{2}\omega^2 a^2 \sin^2\theta - \omega^2 a \;\sin^2\theta\,\delta r = \text{constant}$$

the last term is << the second (see below), so

$$\delta r \simeq \text{ const.} + \frac{\omega^2 a^4}{2GM}\sin^2\theta$$

As expected, the ocean surface is flattened at the poles. The oblateness of the ocean surface is defined as

$$\varepsilon = \frac{r_{eq} - r_{pole}}{r_{eq}}$$

i.e., $$\varepsilon \simeq \frac{\omega^2 a^3}{2GM} \equiv \frac{1}{2}q$$

Note that the dimensionless ratio q is just the ratio of centrifugal acceleration at the equator to the gravitational acceleration. Our analysis will only be reasonally correct so long as $q << 1$.

Some observed* values of q and ε for planets:

	Earth	Mars	Jupiter
q	0.00346	0.00460	0.08882
½q	0.00173	0.00230	0.04441
ε_{obs}	0.00335	0.0050 (3)	0.0648 (1)

We see that $q \ll 1$ as we assumed above, and that ε and $\frac{q}{2}$ are comparable in size, but that in general ε is 1.5 - 2 times greater than predicted. Why?

The answer is that we have neglected the feedback effect that the rotational distortion has on the planet's gravity field, which is no longer that of a sphere.

[Aside: Rotational disruption.

Clearly a planet becomes severly distorted if q approaches unity. This sets an upper limit on the rotational velocity of a planet. Roughly,

$$\omega_{max} \simeq \left(\frac{GM}{a^3}\right)^{\frac{1}{2}} \sim 2\left(G\bar{\rho}\right)^{\frac{1}{2}}$$

where $\bar{\rho}$ is the planet's average density. For the Earth, $\bar{\rho}$ = 5.52 $g\ cm^{-3}$, so

$$\omega_{max} \simeq 1.2 \times 10^{-3} \text{ rad}\,\text{sec}^{-1}$$

or $P_{min} \simeq 1.4$ hrs.

For Jupiter,

$P_{min} \simeq 2.9$ hrs.]

*values in ( ) are uncertainties in the last figure.

Planetary Gravity Fields

Because of rotational flattening, most planets (but not most satellites) may be treated to a good approximation as oblate spheroids; i.e., ellipsoids with 2 equal long axes and 1 short axis. A basic result of potential theory is that the external potential of any body with an axis of symmetry can be written in the form

$$V_G(r,\theta) = -\frac{GM}{r}\left\{1 - \sum_{n=2}^{\infty} J_n \left(R/r\right)^n P_n(\mu)\right\}$$

where M = total mass

R = equatorial radius

J_n = dimensionless constants

$P_n(\mu)$ = Legendre polynomial of degree n

$\mu = \cos\theta$

(Note that there is no n = 1 term, as long as the origin of co-ordinates is chosen as the body's center of mass.)

The first few P_n's are:

$$P_0(\mu) = 1$$

$$P_1(\mu) = \mu$$

$$P_2(\mu) = \frac{1}{2}\left(3\mu^2 - 1\right)$$

$$P_3(\mu) = \frac{1}{2}\left(5\mu^3 - 3\mu\right)$$

$$P_4(\mu) = \frac{1}{8}\left(35\mu^4 - 30\mu^2 + 3\right).$$

The J_n's reflect the distribution of mass within the body, and must be determined empirically for a planet. J_2 is by far the most important, and has a simple physical interpretation in terms of the polar (C) and equatorial (A) moments of inertia:

$$J_2 = \frac{C - A}{MR^2}$$

[In general, J_n is given by the integral

$$J_n = -\frac{1}{MR^n}\int_0^R\int_{-1}^{-1} r^n P_n(\mu)\,\rho(r,\mu)\,2\pi\, r^2 d\mu\, dr$$

where $\rho(r,\mu)$ is the internal density distribution. Since $P_n(\mu)$ is an odd function for odd n, $J_3 = J_5 = J_7 = \cdots = 0$ for a planet whose northern and southern hemispheres are symmetric. In fact, only the Earth has a measured non-zero value of J_3.]

Relation between rotation, J_2, and oblateness

Let us now return to the question of the oblateness of a rotating planet, including the effect of the non-spherical gravity field. Recall that the centrifugal potential is given by

$$V_c = -\frac{1}{2}\omega^2 r^2 \sin^2\theta$$
$$= \frac{1}{3}\omega^2 r^2\left(P_2(\mu) - 1\right)$$

We can ignore the term which is independent of μ, so V_c has the same angular dependence as the J_2 term in the planetary gravity field. The total potential at the surface of the planet is

$$V_T(r,\theta) = V_G(r,\theta) + V_c(r,\theta)$$
$$= -\frac{GM}{r} + \left[\frac{GMR^2}{r^3}J_2 + \frac{1}{3}\omega^2 r^2\right]P_2[\mu]\,*$$

where we neglect J_4, J_6 etc.

As before, we require the surface to be an equipotential (this is true even for solid planets) and write $r = R + \delta r(\theta)$:

$$\delta r = const. - \left[J_2 + \frac{1}{3}q\right]R\,P_2(\mu)$$

Relation of J_n to rotation rate

The connection between J_2, J_4, J_6, … and the rotation rate is not straightforward to derive, involving a self-consistent solution along the lines:

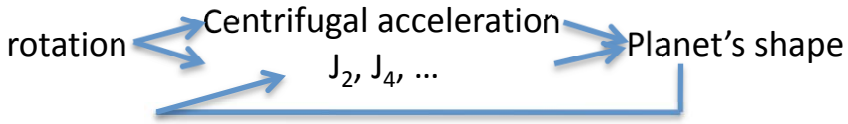

So long as the rotation parameter, q, is small, it can be shown that

$$J_n \propto q^{n/2}$$

Where the proportionality constants are usually of order unity. Since $q << 1$ generally, the higher-order J_n's rapidly become small. For J_2, the above relation is usually written

$$J_2 = \frac{1}{3} k_2 q \quad (\text{*Note that } V_{J_2}/V_c = 3J_2/q = k_2, \text{ which is the real definition of } k_2.)$$

and k_2 is known as a 2nd order Love number.

With k_2 defined this way, we have $q = 3J_2$, i.e., $V_{J_2} = V_c$, when $k_2 = 1$

For a uniform density planet it can be shown that

$$k_2 = 3/2$$

$$\text{so } J_2 = q/2 .$$

Examples of Planetary J_n's and k_2's:

		Earth	Mars	Jupiter
J_2	10^{-6}	1083	1956	14733
J_3	10^{-6}	−2.5	33	≤ 50
J_4	10^{-6}	−1.6	−18	−587
$k_2 = 3J_2/q$		0.94	1.28	0.50
J_4/q^2		0.13	0.85	0.074

Note that the expression for J_n on the previous slide implies that J_n becomes smaller as the mass of the planet is more concentrated toward the center. Based on the values for k_2 in the Table, we conclude that Jupiter is the most centrally-concentrated, and Mars the least. Even Mars, however, has a k_2 appreciably less than that of a uniform-density planet, i.e., 1.50.

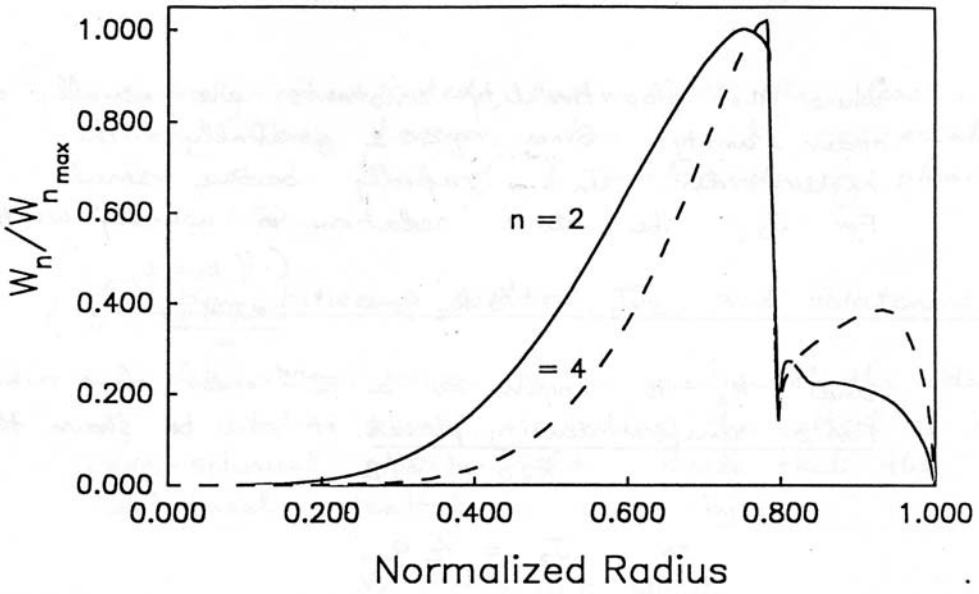

Weighting functions for J_n: $r^{n+2}\,\rho(r)$ (Uranus)

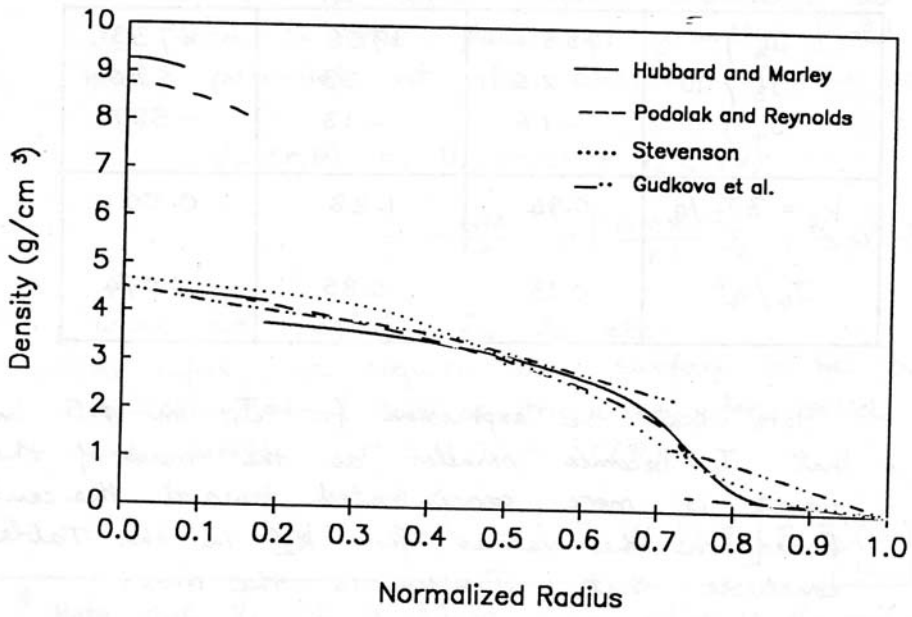

Let's return to the question of the planet's equilibrium shape:

Since $P_2(\mu)$ varies from 1.0 at the poles $(\mu = \pm 1)$ to -0.5 at the equator $(\mu = 0)$ the planet's oblateness is

$$\varepsilon = \frac{r_{eq} - r_{pole}}{r_{eq}}$$

i.e., $\boxed{\varepsilon = \frac{3}{2} J_2 + \frac{1}{2} q}$

(This replaces our earlier result, $\varepsilon = \frac{1}{2} q$.)

For our hypothetical uniform-density planet,

$$J_2 = \frac{1}{2} q, \text{ so}$$

$$\varepsilon = \frac{5}{4} q.)$$

In general, in terms of the Love number $k_2 = 3\frac{J_2}{q}$, we have

$$\varepsilon = (1 + k_2)\frac{q}{2}$$

$$\equiv h_2 \frac{q}{2}, \qquad \boxed{\text{k}_2 \text{ is the "response coefficient" of the planet to } V_c}$$

where we introduce another Love number, h_2. As we have shown, for a planet in hydrostatic equilibrium,

$h_2 = 1 + k_2$

Let's compare the observed oblateness with this result (note that if both J_2 and q are known for a planet, no further knowledge of the planet's density distribution is needed to predict ε):

	Earth	Mars	Jupiter
q	0.00346	0.00460	0.08882
J_2	0.00108	0.00196	0.01473
$\varepsilon_{pred.}$	0.00335	0.00524	0.06651
$\varepsilon_{obs.}$	0.00335	0.0050 (3)	0.0648 (1)
$h_2 = 2\,\varepsilon/q$	1.94	2.17	1.46
C/MR^2	0.332	0.375	0.259

Voila! – almost perfect agreement with our predicted values, confirming our assumption of hydrostatic equilibrium. In the last line we give the polar moment of inertia factor, $\frac{C}{MR^2}$, derived from these observational values. This is an important constraint on planetary interior models, and is obtained from the approximate formula, derived by Clairaut

$$h_2 \simeq \frac{5}{1+\left(\frac{5}{2} - \frac{15}{4} \bullet \frac{C}{MR^2}\right)}.$$

(Note that this yields the correct value of $h_2 = 5/2$ for a uniform density planet with $c = 2/5\ MR^2$; but gives $h_2 = 20 / 29/$ for $C = 0$, rather than the correct value of 1.)

Review of Love numbers:

centrifugal potential, $V_c = -\frac{1}{2}\omega^2 r^2 \sin^2\theta$

$$= \frac{1}{3}\omega^2 r^2 \left[P_2\left(\cos\theta\right) - 1 \right]$$

gravitational potential (quadrupole term), $V_2 = \frac{GMR^2}{r^3} J_2 P_2\left(\cos\theta\right)$

potential Love number, $k_2 \equiv \frac{V_2}{V_3}\left(r = R\right)$

$$= 3\left(\frac{GM}{\omega^2 R^3} \right) J_2$$

i.e., $J_2 = \frac{1}{3} k_2 q$

hyrdrostatic figure: $\varepsilon = \frac{1}{2} q \left(1 + \frac{V_2}{V_c} \right)$

$$= \frac{1}{2} q \left(1 + k_2\right)$$

$$\equiv \frac{1}{2} q\, h_2$$

where the shape Love number $h_2 = 1 + k_2$

$$\therefore \quad \varepsilon = \frac{1}{2} q + \frac{1}{2} q\, k_2 q = \frac{1}{2} q + \frac{3}{2} J_2$$

In general, k_2 and h_2 depend on the internal density profile $\rho\left(r\right)$. For a reasonably uniform planet, Clairaut &Radau showed that:

$$h_2 = 1 + k_2 \simeq \frac{5}{1 + \left(5/2 - 15/4 \;\; C/MR^2 \right)^2}$$

if ρ = constant, $\frac{C}{MR^2} = \frac{2}{5}$ and we have:

$$h_2 = \frac{5}{2}, \; k_2 = \frac{3}{2}$$

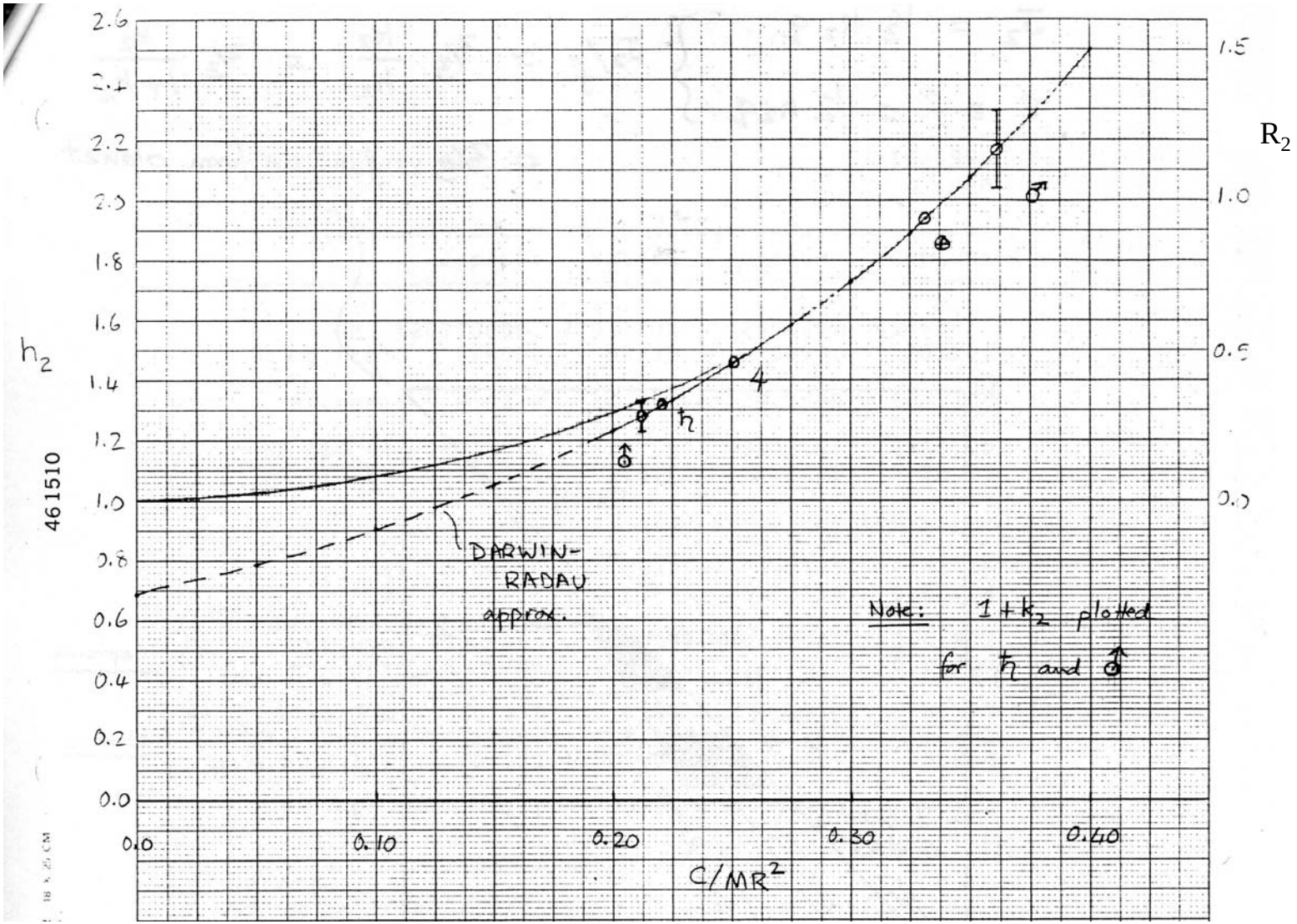
h_2
R_2
461510
2.6
2.4
2.2
2.0
1.8
1.6
1.4
1.2
1.0
0.8
0.6
0.4
0.2
0.0
1.5
1.0
0.5
0.0
0.0
0.10
0.20
0.30
0.40
C/MR^2
DARWIN-
RADAU
approx.
Note: $1+k_2$ plotted
for ♄ and ♁
♄
4
♁
♂

$$\left.\begin{aligned} J_2 &\simeq \frac{1}{3}k_2 q \\ \varepsilon \equiv f &\simeq \frac{1}{2}h_2 q \end{aligned}\right\} \frac{J_2}{f} \simeq \frac{2}{3}\frac{k_2}{h_2} = \frac{2}{3}\frac{k_2}{1+k_2} = \frac{2}{5} \text{ for uniform planet}$$

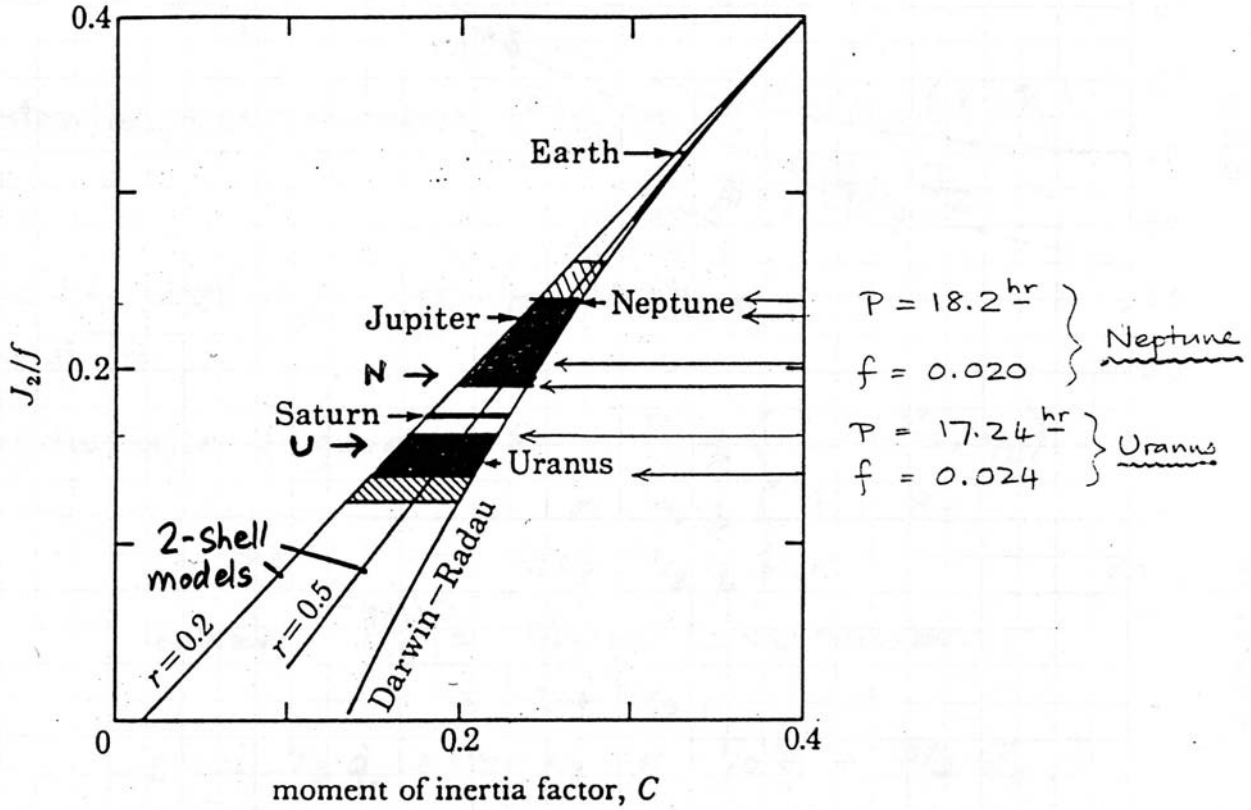

1. Bounds on the moment of inertia factors C can be estimated from the observed values of J_2/f. Independent any interior model, we can state that Saturn is more centrally condensed than Jupiter and that Uranus is obably the most centrally condensed planet in the Solar System. The oblateness f of Neptune is calculated om J_2, $\langle\rho\rangle$ and T ($= 18.2 \pm 0.4$ h: see table 1), and the same procedure has been followed for Jupiter and turn. It would appear that Neptune and Uranus have quite different interiors.

Figure after Dermott (1984)

D-R relation: $\frac{J_2}{f} = \frac{8}{15} - \frac{5}{6}\left(1 - \frac{3}{2}\frac{C}{MR^2}\right)^2$

Planetary figures. 2/15/1990
pdn

	Jupiter	Saturn	Uranus	Neptune
GM	126776000.	37931200.	5793939.	6835096.
R_eq (km)	71400.	60330.	26200.	25225.
P (hrs)	9.9249	10.6567	17.2400	16.1100
J2 (10^6)	14733.00	16297.00	3343.43	3411.00
J4 (10^6)	-587.00	-910.00	-28.85	-26.00
q	0.08879	0.15528	0.03181	0.02756
m	0.08288	0.13943	0.03115	0.02704
eps_dyn	0.06458	0.09589	0.02067	0.01872
eps_opt	0.06480	0.09820	0.02000	0.01800
k2=3J2/m	0.533	0.351	0.322	0.378
h2=2eps/m	1.564	1.409	1.284	1.331
L4=J4/q^2	-0.074	-0.038	-0.029	-0.034
C/MR^2	0.271	0.241	0.213	0.224

Notes:
GM in km^3/sec^2
P = magnetic field rotation period = 2*pi/w
q = w^2*R_eq^3/GM
m = w^2*R_av^3/GM = q*(1-eps_dyn)
C/M*R^2 calculated from the Darwin-Radau relation,
using m and eps_opt.
h2 calculated using eps_opt, not eps_dyn
L4 = 4th order response coefficient

Experimental Determination of ω, J_2, and ε

Rotation Rate, ω

Interior rotation rate:

Magnetic field rotation via radio emission

Surface/atmospheric rotation rates:

Feature tracking (surfaces & clouds)

Doppler Shifts (radar)

Gravity Field: *GM*, J_2, J_4, etc.

Natural satellites:

Periods & semi-major axes $\Rightarrow GM$

$\dot{\tilde{\omega}}$ & $\dot{\Omega}$ vs. $a \Rightarrow J_2, J_4$

Rings

$\dot{\tilde{\omega}}$ & $\dot{\Omega}$ vs. $a \Rightarrow J_2, J_4, J_6$

resonance locations $\Rightarrow GM, J_2$

Spacecraft:

Doppler tracking $\Rightarrow GM, J_2, J_4$

Oblateness, ε:

Solid surface/cloud tops:

Imaging (Earth-based or s/c)

Surface pressure variations

Radio occultations

Upper atmosphere

Radio occultations (p ~ 100 mb)

Stellar occulations (1 μb < p < 1 mb)

	T_{ROT}	ε	Method
Mercury[1]	58.65 ± 0.25^{d}	~0°	Radar
	58.661 ± 0.017	~0°	Mariner 10
Venus [2]	243.01 ± 0.03^{d}	177°.4	Radar
Earth	$23^{h}\ 56^{m}\ 04.1^{s}$	23°.45	
Mars	$24^{h}\ 37^{m}\ 22.7^{s}$	25°.19	Optical, Viking
Jupiter	$9^{h}\ 55^{m}\ 29.71^{s}$	–	Radio*
	$9^{h}\ 50^{m} – 9^{h}\ 55^{m}$	3°12	Optical
Saturn	$10^{h}\ 39^{m}\ 24^{s}$	–	Radio
	$10^{h}\ 14^{m} – 10^{h}\ 30^{m}$	26°73	Optical
Uranus	16.2 ± 0.3^{h}	97°65	Optical/Spect.
	15.6 ± 1.4^{h}	–	J_2 - f
	17.24^{h}	–	Radio
Neptune	18.2 ± 0.4^{h}	29°36	Optical
	14.9 ± 1.6^{h}	–	J_2 - f
	16.11^{h}	–	Radio
Pluto	6.3867^{d}	~118°	Photometric

(1) Mercury's spin is in a 3:2 resonance with its orbit.

(2) Venus' spin (solar day) is near a 5:1 resonance with Earth conjunction, though this may be coincidence.

*Cassini results suggest a longer, and variable, period

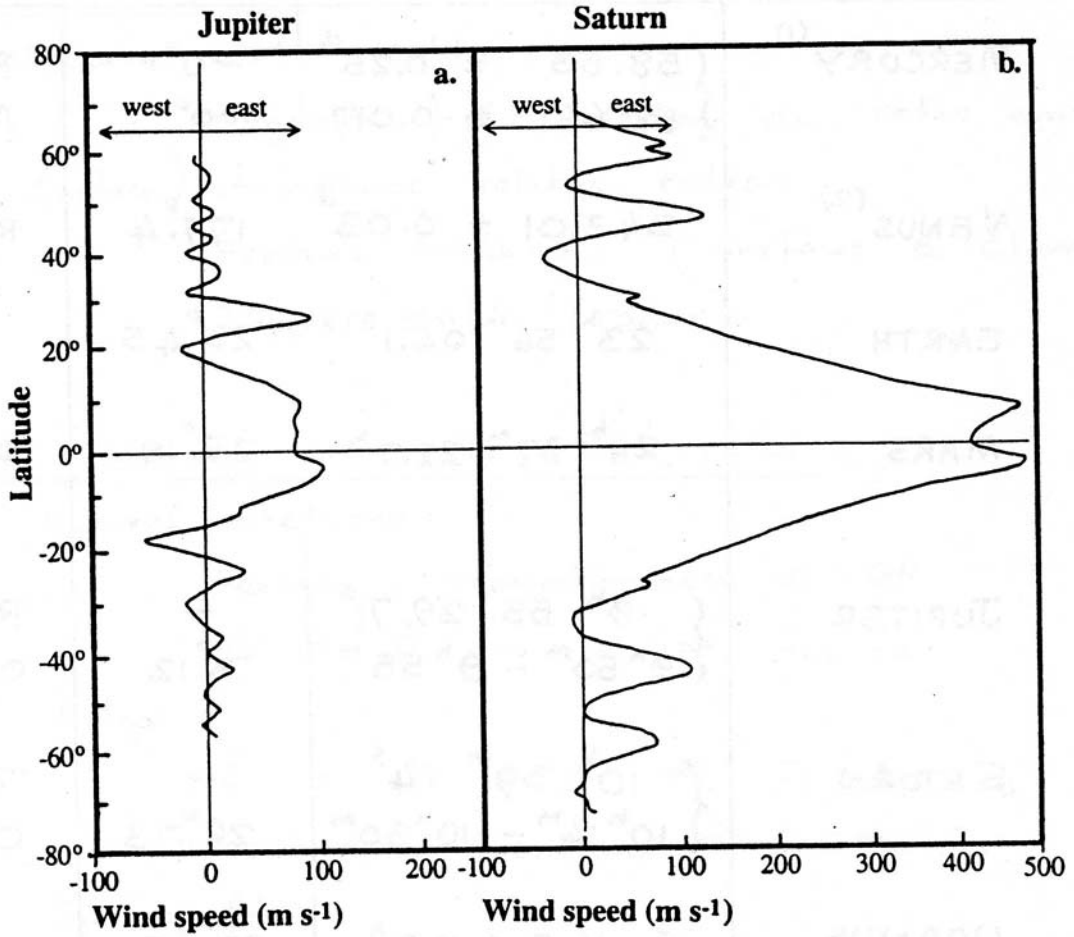

Figure V.28 Speeds of currents in the atmospheres of Jupiter and Saturn. The speeds of currents deduced from the motions of observed bright spots on Jupiter (the east–west or *zonal* wind speeds) are shown in a. b uses the far smaller data set on spot motions on Saturn to construct a similar figure.

Lewis 1995

-Voyager measurements (1979 – 1981)

Note that “0” wind speed is measured wrt the radio (System III) rotation period, which is assumed to match the magnetic field and thus the interior rotation period.

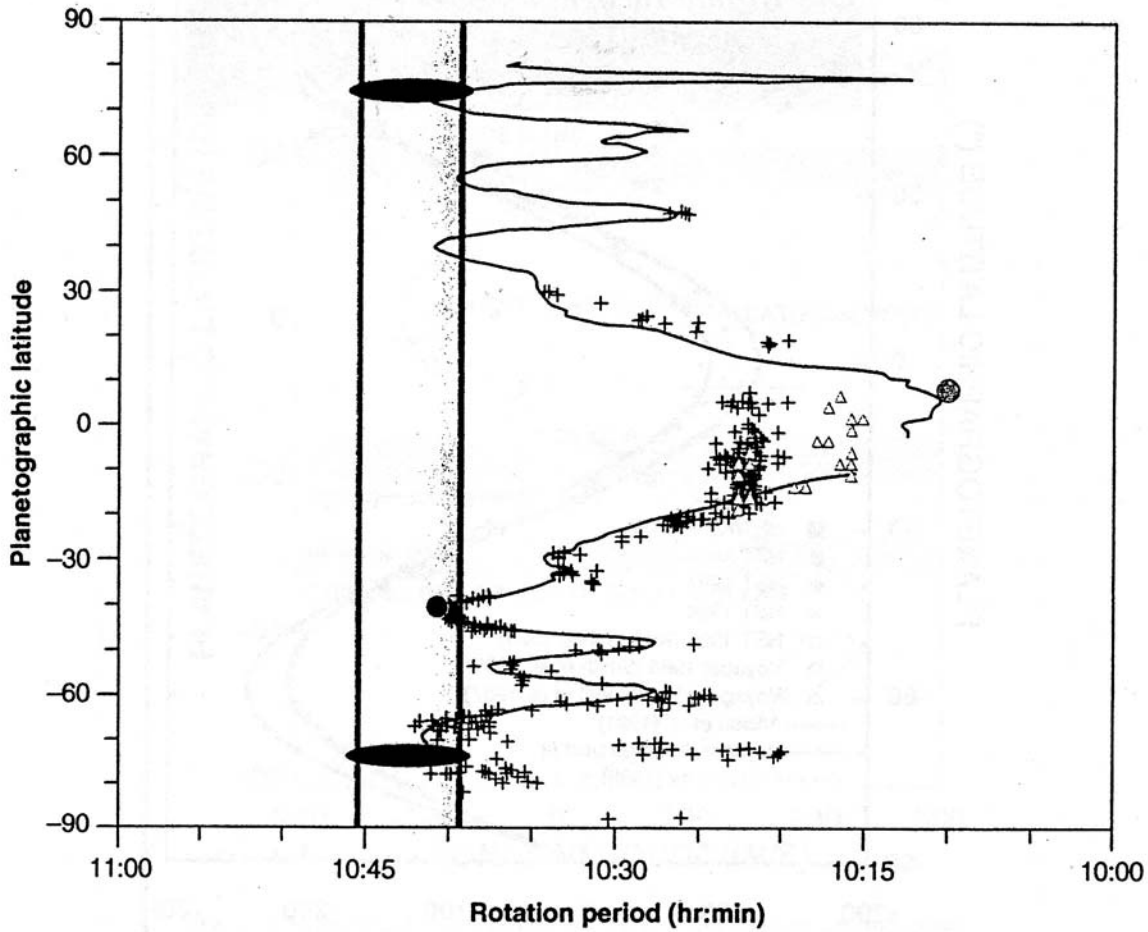

Fig. 1. Saturn's rotation periods. Cloud tracking of atmospheric features, as measured during the Voyager 1 and 2 encounters in 1980 and 1981, are represented by a dark continuous line (*15*). Violet crosses mark points measured from 1994 to 2004 with the Hubble Space Telescope (*9*). Yellow triangles are the equatorial data measured by Cassini (*10*). Outside the equator, the Voyager, Hubble, and Cassini data essentially coincide. The dots indicate short radio emission bursts that have been assigned to lightning produced by storms [yellow dot, Voyager (*16*); red dot, Cassini (*1*, *10*)]. The brown vertical line is the SKR emission period from Voyager (*3*, *4*, *6*), the green vertical line is the SKR emission as measured by Cassini (*1*), and the shaded area indicates the periods determined by the Ulysses spacecraft (*2*). The blue ovals indicate the approximate latitudes of the SKR emissions.

Sanchez-Lavega (2005) Science **307**, 1223.

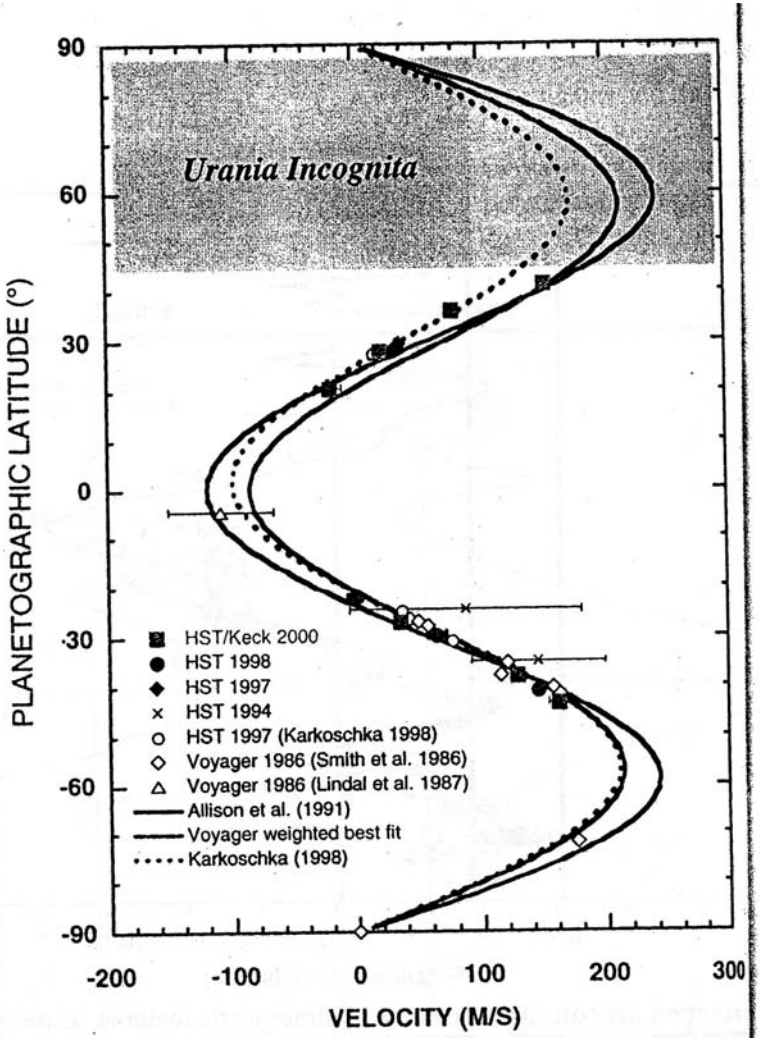

FIG. 2. Zonal velocities of winds on Uranus. The data are shown in Table II, where the velocities are also converted to rotation periods as a function of latitude. Points marked with "x" were obtained using HST in 1994, solid symbols are from 1997 (blue), 1998 (green), and 2000 (red). Open symbols were obtained from Voyager in 1986 (diamonds—Smith *et al.* 1986; the diamond at −90° represents an assumption of zero velocity at the pole; triangle—Lindal *et al.* 1986) and from HST in 1997 (circles—Karkoschka 1998). When not visible, error bars are smaller than the points shown. Three models are shown: the published approximation of Allison *et al.* (1991) to Voyager data (solid black line); a more rigorous fit to the Voyager data weighting the data with their errors (solid purple line); and Karkoschka's (1998) asymmetric fit (black dashed line). We have not yet had adequate spatial resolution northward of 45° to track features (see Fig. 2).

Hammel et al., (2001) Icarus **153**, 229

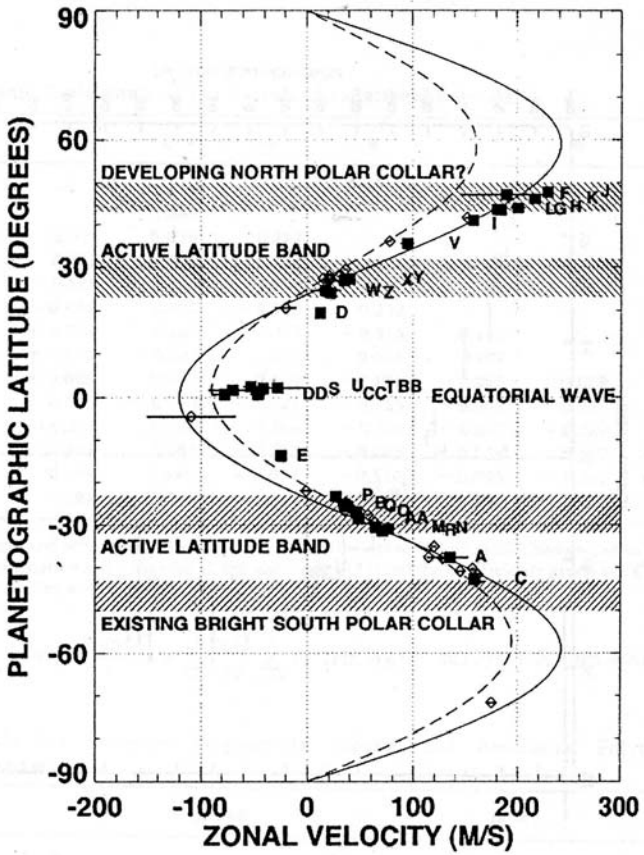

Fig. 2. Uranus zonal wind profile in 2003. Solid squares are the points listed in Table 3; open symbols are past measurements from HST, Keck, and Voyager (no systematic differences are seen as a function of observation wavelength; see Table II in Hammel et al., 2001). The 2003 letter labels are offset to the right for clarity. All points are shown with error bars, though the errors are often smaller than the size of the points. The large error bars on the 2003 equatorial features are indicative of their diffuse nature, which makes defining their locations challenging. To within the measurement errors, they have similar zonal velocities, and in fact may be a manifestation of a wave pattern (see discussion in Section 3). The hatched region from $-50°$ to $-43°$ corresponds to the bright polar collar clearly evident at J and H (Fig. 1). The hatched region from $+43°$ to $+50°$ mirrors the southern latitudes values. Many of the northern features are clustered at these latitudes (see "symmetry" discussion in Section 4). The hatched region from $-32°$ to $-23°$ was defined to enclose most of the southern mid-latitude features seen in the 2003 data and the earlier measurements. The symmetric band in the north, from $+23°$ to $+32°$, encloses many of the northern features. The lines indicate models: solid—non-weighted fit to Voyager data (Allison et al., 1991); dotted—asymmetric model of Karkoschka (1998).

Hammel et al., (2000) Icarus **175**, 534

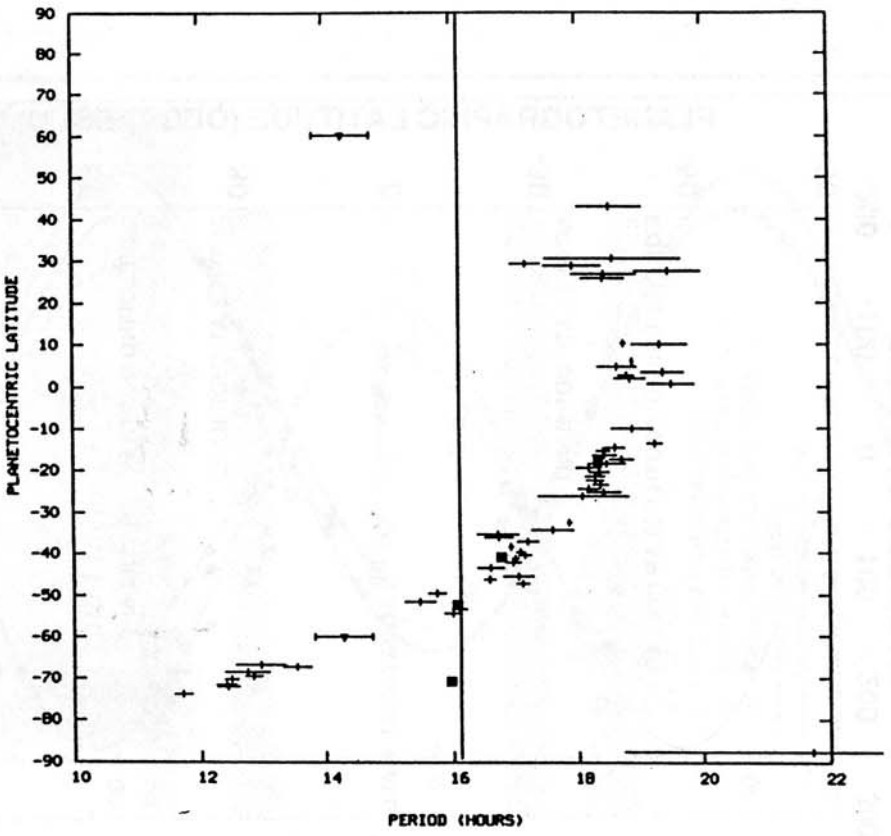

Fig. 7. Rotational periods corresponding to bin-averaged cloud motions. Also shown are the long-term tracking results of the major features (GDS, Scooter, DS2, and the SPFs) reported by *Hammel et al.* [1989a] (squares) and the 60°N 1-bar level zonal wind inferred from radio occultation measurements [*Lindal et al.*, 1990] (inverted triangle), which has also been reflected at 60°S for the sake of comparison.

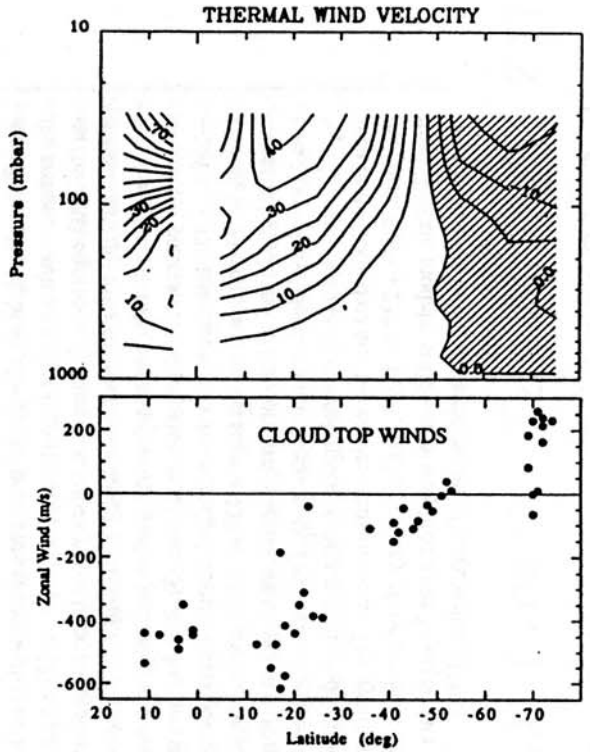

Fig. 5. (Upper panel) Meridional cross section of thermal wind velocity calculated from the temperature structure of Figure 4 and assuming zero wind speed at the 1000-mbar level. The velocity is expressed in meters per second with positive numbers indicating an eastward flow while negative numbers denote westward winds (hatched area). (Lower panel) Winds obtained from tracking cloud features [*Smith et al.*, 1989].

Table 4.1 Harmonic Coefficients of the Earth's Gravitational Potential*

l \ m	0	1	2	3	4	5	6	7	8
2	− 484.172	—	2.426						
			− 1.386						
3	0.958	2.017	0.919	0.719					
		0.251	− 0.617	1.420					
4	0.547	− 0.532	0.354	0.974	− 0.167				
		− 0.444	0.662	− 0.220	0.312				
5	0.068	− 0.069	0.657	− 0.472	− 0.315	0.149			
		− 0.082	− 0.317	− 0.231	0.028	− 0.679			
6	− 0.161	− 0.089	0.068	0.017	− 0.101	− 0.293	0.038		
		− 0.020	− 0.368	− 0.024	− 0.453	− 0.508	− 0.230		
7	0.092	0.252	0.339	0.259	− 0.270	− 0.007	− 0.329	0.065	
		0.131	0.085	− 0.216	− 0.086	0.053	0.150	0.036	
8	0.062	0.024	0.049	− 0.024	− 0.240	− 0.093	− 0.037	0.051	− 0.091
		0.092	0.066	− 0.074	0.068	0.084	0.301	0.073	0.097

*Coefficients to degree and order (8, 8) from the more extensive set of Rapp (1973). These refer to the fully normalized harmonic functions p_l^m defined in Appendix C. For each value of (l, m) the coefficients given are $\bar{C}_l^m$ followed by $\bar{S}_l^m$ in units of 10^{-6}. Uncertainties are of order 0.02.

$$V = -\frac{GM}{r}\left\{1 + \sum_{l=2}^{\infty}\left(\frac{a}{r}\right)^l \sum_{m=0}^{l} P_l^m(\sin\phi)[C_l^m \cos m\lambda + S_l^m \sin m\lambda]\right\}$$

Table C.1 Legendre Polynomials $P_l(\cos\theta)$ and Associated Polynomials $P_l^m(\cos\theta)$*

	$m = 0$	$m = 1$
$l = 0$	$1\,(1)$	—
1	$\cos\theta\,(\sqrt{3})$	$\sin\theta\,(\sqrt{3})$
2	$\frac{1}{2}(3\cos^2\theta - 1)\,(\sqrt{5})$	$3\cos\theta\sin\theta\,(\sqrt{5/3})$
3	$\frac{1}{2}(5\cos^3\theta - 3\cos\theta)\,(\sqrt{7})$	$\frac{3}{2}(5\cos^2\theta - 1)\sin\theta\,(\sqrt{7/6})$
4	$\frac{1}{8}(35\cos^4\theta - 30\cos^2\theta + 3)(\sqrt{9})$	$\frac{5}{2}(7\cos^3\theta - 3\cos\theta)\sin\theta\,(\sqrt{9/10})$

	$m = 2$	$m = 3$	$m = 4$
$l = 0$	—	—	—
1	—	—	—
2	$3\sin^2\theta\,(\sqrt{5/12})$	—	—
3	$15\cos\theta\sin^2\theta\,(\sqrt{7/60})$	$15\sin^3\theta\,(\sqrt{7/360})$	—
4	$\frac{15}{2}(7\cos^2\theta - 1)\sin^2\theta\,(\sqrt{1/20})$	$105\cos\theta\sin^3\theta\,(\sqrt{1/280})$	$105\sin^4\theta\,(\sqrt{1/2240})$

*Factors in brackets convert P_l^m to p_l^m by Equation C.14.

$$p_l^m(\cos\theta) = \left[(2 - \delta_{m,0})(2l+1)\frac{(l-m)!}{(l+m)!}\right]^{1/2} P_l^m(\cos\theta)$$

which is so defined that

$$\frac{1}{4\pi}\int_0^{2\pi}\int_{-1}^{1} \{p_l^m(\cos\theta)[\sin m\lambda, \cos m\lambda]\}^2\, d(\cos\theta)\, d\lambda = 1$$

F. Stacey: “Physics of the Earth”

TABLE 2. Spherical Harmonic Coefficients for the Gravity Field of Mars (Normalized)

L	M	$C(L, M) \times 10^6$	$S(L, M) \times 10^6$	L	M	$C(L, M) \times 10^6$	$S(L, M) \times 10^6$	L	M	$C(L, M) \times 10^6$	$S(L, M) \times 10^6$
2	0	−876.19994		10	3	−1.66385	0.77579	11	8	0.53943	4.19394
3	0	−11.17932		11	3	−1.47778	−4.17005	12	8	0.11698	−0.82392
4	0	3.39646		12	3	2.38075	−0.74525				
5	0	1.94782									
6	0	0.95118		4	4	−0.86685	−13.47390	9	9	−2.40589	0.51106
7	0	−0.64397		5	4	−6.11579	−2.08040	10	9	−2.90963	−3.69136
8	0	−0.07718		6	4	2.11695	1.29677	11	9	−3.44076	0.46914
9	0	−2.35474		7	4	2.57337	0.60075	12	9	0.99384	−0.68860
10	0	−1.69819		8	4	−0.56278	3.04243	10	10	0.20097	−0.11902
11	0	−1.32526		9	4	−1.82713	−1.82521	11	10	0.18630	0.91055
12	0	−0.75032		10	4	2.17118	−1.10625	12	10	2.53626	1.32534
				11	4	−1.74195	0.86302				
3	1	4.53923	24.27684	12	4	−3.15088	0.95681	11	11	3.18144	2.12870
4	1	2.79383	4.96864					12	11	3.69804	−4.53302
5	1	1.50057	4.39836	5	5	−4.19976	2.68363				
6	1	5.79006	−5.06255	6	5	1.81157	2.88149	12	12	0.46169	3.23248
7	1	−4.68089	5.71551	7	5	0.87602	−1.82104				
8	1	3.17404	−6.68414	8	5	−7.67396	−1.48639				
9	1	−0.00391	0.00145	9	5	5.64058	−4.04659				
10	1	−2.53042	3.66725	10	5	−2.12529	3.86293				
11	1	−0.43072	−3.17273	11	5	−0.89633	−2.40769				
12	1	−1.79823	−1.81442	12	5	4.05614	2.98713				
2	2	−85.08972	48.48551	6	6	3.84012	1.53931				
3	2	−17.17102	9.05034	7	6	−1.05321	−3.23803				
4	2	−1.55370	−9.81689	8	6	−1.19139	−0.58019				
5	2	−3.63391	−1.79627	9	6	2.29895	−3.03875				
6	2	2.90876	1.72510	10	6	0.15382	3.27933				
7	2	1.35831	2.53353	11	6	−1.52224	−1.31639				
8	2	3.91598	−1.75760	12	6	0.66204	−3.39938				
9	2	5.46435	−0.96986								
10	2	1.49405	3.20310	7	7	0.37316	−3.20110				
11	2	0.75626	1.49371	8	7	−1.92550	2.61934				
12	2	1.71470	−0.94399	9	7	1.83141	1.70025				
				10	7	−2.56323	−0.53173				
3	3	34.90951	25.60092	11	7	5.97213	−0.16338				
4	3	5.98673	1.33496	12	7	−1.99983	2.73047				
5	3	4.44513	2.55021								
6	3	−0.12124	−0.39408	8	8	−1.18752	−0.55463				
7	3	4.43077	4.46684	9	8	1.52922	1.67698				
8	3	−4.12814	−2.36553	10	8	1.91090	−0.30612				
9	3	3.67050	1.62755								

Mariner 9 + Viking orbiters

JGR 84, 7943 (1979)

JGR 85, 8303 (1980)

TABLE 2. Sixth-Degree and Sixth Order Unnormalized Harmonic Coefficient Estimates and Their Uncertainties

l	m	C_{lm}	$\sigma_{C_{lm}}$	S_{lm}	$\sigma_{S_{lm}}$
2	0	−0.597E−5*	0.32E−5		
2	1	0.640E−8	0.11E−5	−0.299E−6	0.13E−5
2	2	−0.332E−6	0.81E−6	−0.174E−5	0.74E−6
3	0	0.779E−5	0.73E−5		
3	1	0.191E−5	0.26E−5	0.985E−6	0.24E−5
3	2	−0.175E−6	0.51E−6	0.438E−6	0.56E−6
3	3	−0.150E−7	0.15E−6	0.413E−7	0.13E−6
4	0	−0.165E−5	0.42E−5		
4	1	−0.198E−6	0.14E−5	0.127E−6	0.14E−5
4	2	0.421E−6	0.33E−6	0.220E−6	0.33E−6
4	3	−0.560E−7	0.54E−7	−0.234E−7	0.56E−7
4	4	−0.179E−7	0.15E−7	0.173E−8	0.14E−7
5	0	−0.691E−6	0.32E−5		
5	1	−0.379E−7	0.84E−6	0.404E−8	0.84E−6
5	2	0.156E−7	0.16E−6	0.925E−7	0.16E−6
5	3	0.115E−7	0.30E−7	−0.541E−8	0.29E−7
5	4	0.743E−8	0.52E−8	0.296E−8	0.54E−8
5	5	0.102E−8	0.13E−8	−0.163E−8	0.14E−8
6	0	−0.424E−6	0.24E−5		
6	1	−0.180E−7	0.54E−6	0.546E−8	0.54E−6
6	2	0.711E−8	0.85E−7	0.159E−7	0.85E−7
6	3	0.152E−9	0.14E−7	0.225E−8	0.14E−7
6	4	0.404E−11	0.33E−8	0.179E−8	0.23E−8
6	5	0.305E−10	0.41E−9	−0.138E−9	0.38E−9
6	6	−0.120E−9	0.91E−10	−0.109E−9	0.89E−10

* Read −0.597E−5 as -0.597×10^{-5}

The derived gravity field assumes the spherical harmonic representation of the gravity potential and is expressed as

$$U(r, \phi, \lambda) = \frac{\mu}{r}\left\{1 + \sum_{l=2}^{n}\sum_{m=1}^{l}\left(\frac{R_e}{r}\right)^l P_{lm}(\sin\phi)[C_{lm}\cos m\lambda + S_{lm}\sin m\lambda]\right\} \quad (11)$$

where U is the potential, r is the radius at which the potential is evaluated, ϕ is the latitude, λ is the Venus referenced longitude measured from the prime meridian, l and m are the degree and order of the harmonic coefficients, P_{lm} is the associated Legendre polynomial, μ is the gravitational constant times the Venus mass, C_{lm} and S_{lm} are the harmonic coefficients which represent the gravity field, and R_e is the mean equatorial radius of Venus.

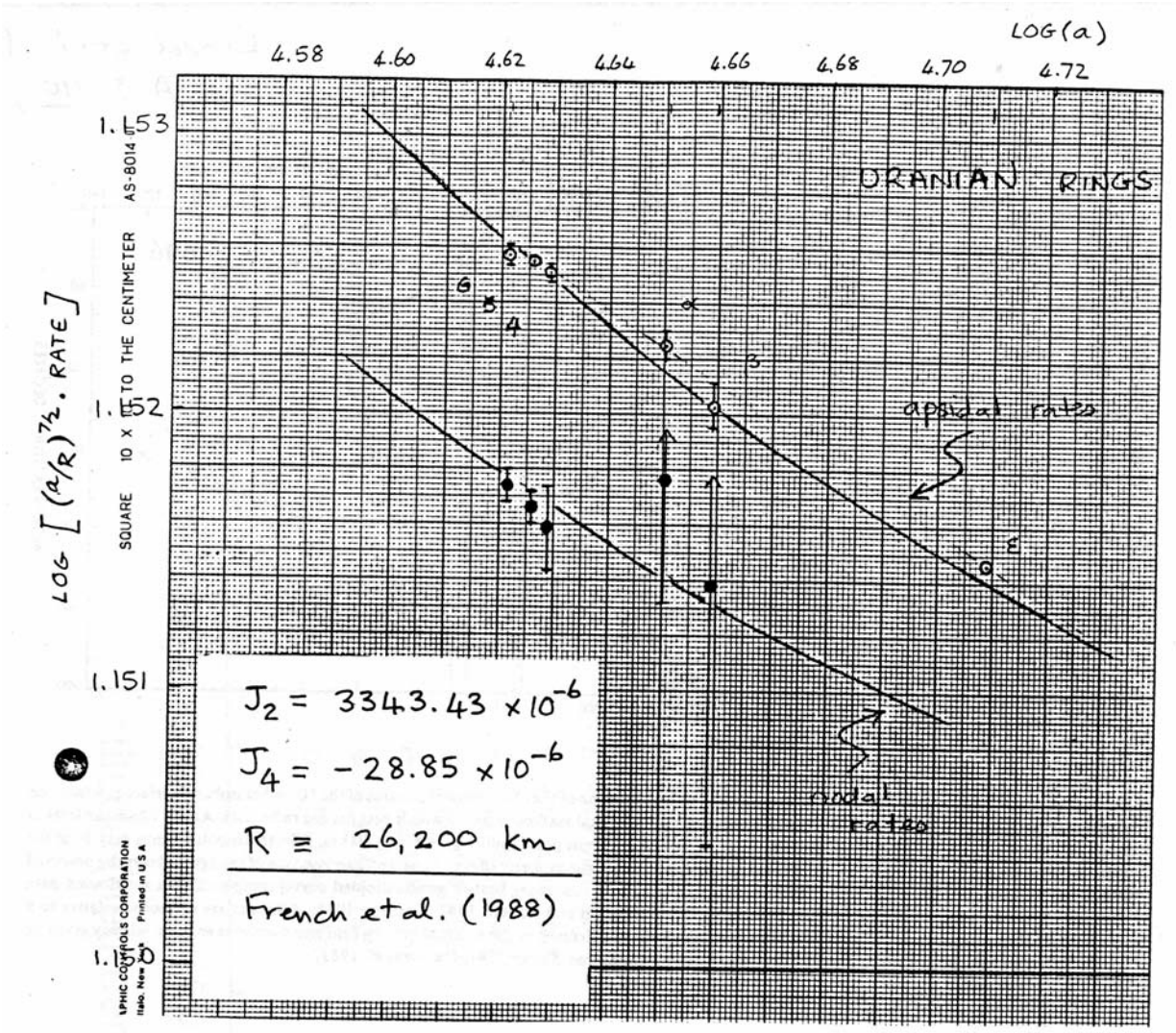

to $0(J_4)$

$$\dot{\bar{\omega}} = \left(\frac{GM}{R^3}\right)^{\frac{1}{2}}\left(\frac{R}{a}\right)^{\frac{7}{2}}\left\{\frac{3}{2}J_2 - \frac{15}{4}J_4\left(\frac{R}{a}\right)^2\right\}$$

$$\dot{\Omega} = -\left(\frac{GM}{R^3}\right)^{\frac{1}{2}}\left(\frac{R}{a}\right)^{\frac{7}{2}}\left\{\frac{3}{2}J_2 - \left[\frac{9}{4}J_2^2 + \frac{15}{4}J_4\right]\left(\frac{R}{a}\right)^2\right\}$$

where a = geometric mean radius

R = planet's equatorial radius

M = planet's mass

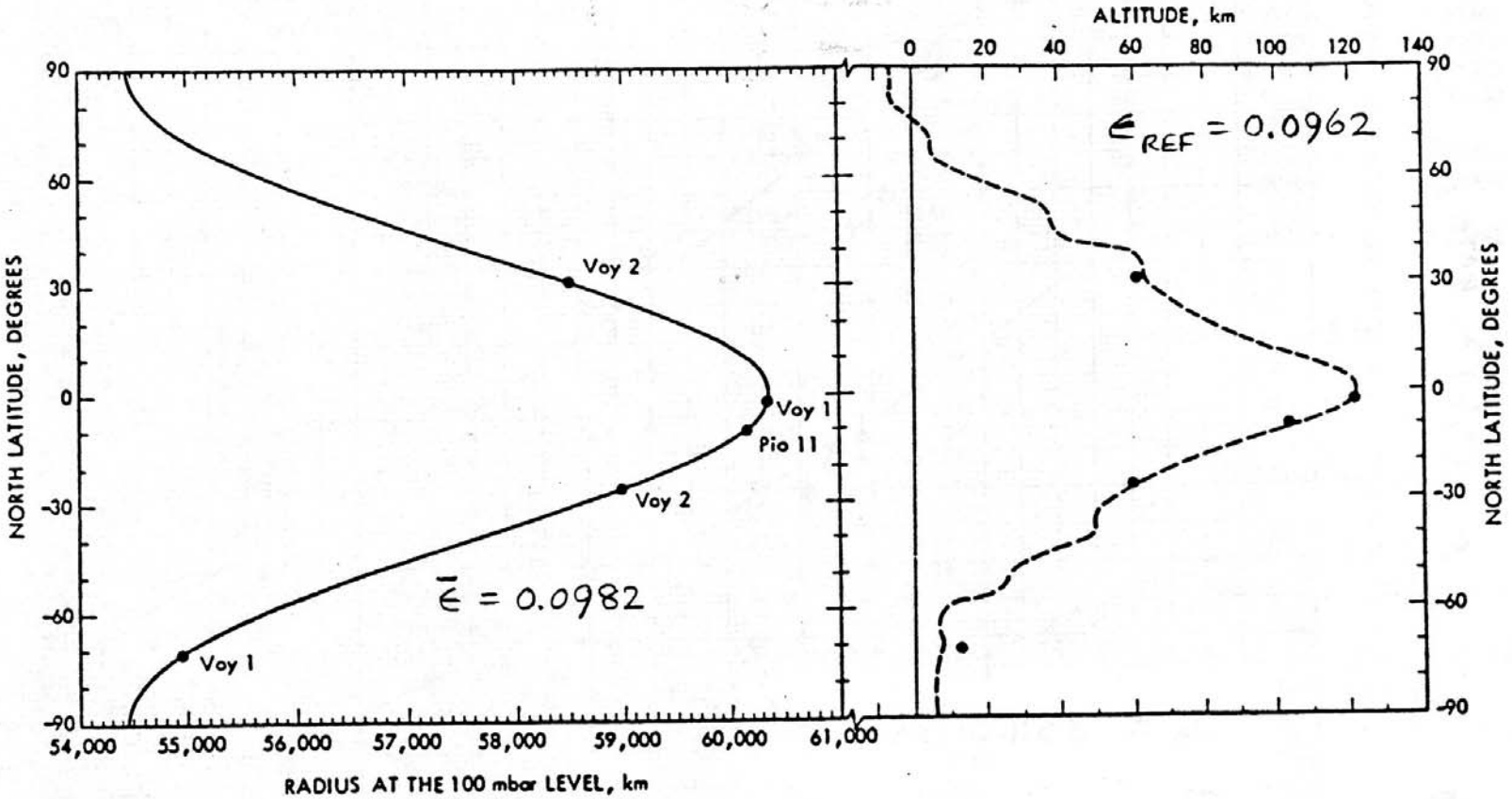

FIG. 9. Saturn's physical shape. The discrete points in the left-hand portion of the chart show the radius of the 100-mbar isobaric surface as a function of planetocentric latitude. The full drawn curve represents the horizontal surface or geoid which best fits the radio data. At the 100-mbar level in Saturn's atmosphere, the equatorial radius is 60 367 ± 4 km and the mean polar radius is 54 438 ± 10 km. (The south-polar radius may be of the order of 10 km greater than the north-polar radius—possibly a seasonal atmospheric effect.) The right-hand portion of the figure shows the observed altitude of the 100-mbar isobaric surface (discrete points) and the corresponding best-fit geoid (stippled curve) computed from zonal-wind data acquired with the Voyager imaging system (Smith *et al.* 1982; Ingersoll and Pollard 1982; Garneau 1984). Altitudes are measured relative to a reference geoid that has a polar radius of 54 438 km and whose shape is defined by the external gravity field and a uniform angular velocity given by the $10^h\ 39^m\ 22.4^s$ magnetic field or system III rotation period (Desch and Kaiser 1981; Davies *et al.* 1983).

Lindal et al. (1985), A.J. **90**, 1136.

Stellar occultation radii